Supporting Information

Kasanetz *et al*. 10.1073/pnas.0711113105

SI Text

Animal Preparation. Adult male Sprague–Dawley rats (n = 36 weight 300–450 g) were maintained on a 12:12 light/dark cycle with food and water available ad libitum and were cared for in accordance with local institutional regulations on the use of laboratory animals (Servicio Nacional de Sanidad y Calidad Agroalimentaria, RS 617/2002, Argentina). On the day of the experiment, the rats were anesthetized with urethane (1.2–1.5 g/kg, i.p.), treated with a local anesthetic on the scalp (bupivacaine hydrochlorate solution, 5% wt/vol, Duracaine, AstraZeneca S.A. Argentina, 0.1–0.3 ml, s.c.) and pressure points (lidocaine hydrochlorate gel, 2% wt/wt, Denver Farma S.A., Argentina), and secured to a stereotaxic frame (Stoelting). Temperature was maintained at 36°C –37°C with a servo-controlled heating pad (Fine Science Tools). Additional urethane was administered throughout the experiment as necessary to maintain a constant level of anesthesia, as determined from cortical LFPs and periodic evaluation of the hindlimb withdrawal reflex (customarily, supplements of 0.3–0.4 g/kg s.c. every 3–4 h) (1, 2). At the end of the recordings, the rats received a lethal dose of urethane and were transcardially perfused with cold saline followed by 4% paraformaldehyde in PBS. Brains were removed, stored overnight in the same fixative, and then incubated in 0.1M PBS containing 15% sucrose for 24–48 h.

Cortical LFP Recordings. Concentric bipolar electrodes (SNE-100, Better Hospital Equipment; shaft contact: ring of 0.25 mm outer diameter, 0.1 mm inner diameter, 0.25 mm height; central contact: exposed wire, 0.25 mm long and 0.1 mm diameter; distance between contacts: 0.75 mm of 0.1 mm diameter isolated wire) were used to obtain differential LFP recordings from separate cortical areas: the medial frontal cortex (3.5 mm anterior to bregma, 0.8 mm lateral to midline and 4 mm below the cortical surface, 20° angle in the sagittal plane; ref. 3), motor cortex (3.2 mm anterior to bregma, 2.5 mm lateral and 2.5 mm below cortical surface, 20° angle in the sagittal plane) and primary somatosensory cortex (2.8 mm posterior to bregma, 6.5 mm lateral and 2 mm below cortical surface, positioned with a 20° angle in the coronal plane; manuscript Fig. 1*A*; ref. 2). Three additional bipolar electrodes were located at a distance of ~0.5 mm from each LFP recording site to deliver electrical stimuli. Responses evoked by cortical electrical stimulation were the subject of a separated study (2) and will not be considered further in the present report. Cortical LFPs were amplified and band-pass filtered (0.1–300 Hz). The localization of LFP recording sites was determined from Nissl-stained sections.

Striatal Intracellular Recording. Intracellular recordings were obtained as described previously (4) from one of the following dorsal striatum territories (ipsilateral to cortical LFP recordings): rostrolateral striatum (0.2–1 mm anterior to bregma, 3–5 mm lateral, 3–5 mm below the cortical surface), rostromedial striatum (+0.4 to –0.2 mm relative to bregma, 1.5–2.5 mm lateral and 3–5 mm below the cortical surface) or caudal striatum (1.3–2 mm posterior to bregma, 3.5–5 mm lateral and 3–5 mm below the cortical surface). Intracellular microelectrodes (60 to 100 MΩ) were filled with 2M potassium acetate and 2% Neurobiotin (RBI). The signal was sent to a bridge amplifier (Axoclamp 2B, Axon Instruments) and digitized at 10 kHz together with the cortical LFPs (DigiData 1322A, Axon Instruments). Microelectrodes were slowly advanced through the striatum with a hydraulic micromanipulator until a neuron was impaled. After completion of experimental procedures, neurons were labeled with Neurobiotin (5). For more details see ref. 4.

Signal Analysis. Recordings lasting >90 seconds and displaying evident cortical slow wave activity were down-sampled to 1000 Hz by averaging 10 successive points to yield a single point (Clampfit 9, Axon Instruments). The V_m of MSNs during UP and DOWN states was estimated from histograms displaying the amount of time spent at any given V_m (all-points histograms, 1 mV resolution; Clampfit 9). Histograms were fitted a dual-Gaussian function and the mode inside each Gaussian was taken as representative of the steady state reached during the DOWN and UP states (4). Input resistance was measured at the steady state response to small hyperpolarizing and depolarizing current pulses (0.4 nA, 100 ms) applied during DOWN states.

Functional connectivity was first assessed by means of spectral analysis and coherence estimation. Fast Fourier Transforms were computed for 6 second long Hanning sliding windows with 75% overlap. Auto- and cross-spectral densities and phase spectra were calculated for each window and averaged, and the resulting spectra were normalized to the total power within the frequency range 0–10 Hz (resolution: 0.17 Hz). Finally, a single coherence spectrum per pair of signals (V_m versus each cortical LFP, LFP versus LFP) was calculated from the average cross-spectral density between the two signals normalized by the average spectral density of each signal. Significant peaks in average auto- and cross-spectra were detected as power values exceeding percentile 95 of the distribution. To compare coherence between MSN-LFP pairs, a single value per MSN-LFP coherence spectrum was obtained by averaging coherence within the frequency range where the cross-spectrum reached significance. Phase lags were determined from portions of phase spectra showing lineal changes in phase angle within the frequency range of synchronous oscillatory activity (6).

Then we investigated phase synchronization between MSNs and cortical LFPs during transitions to the UP and DOWN state. In contrast to coherence, phase synchrony analysis allows studying phase relationships independently of changes in signal amplitudes and with high temporal resolution. Phase synchrony analysis is usually performed in three steps (7): first, signals are band-pass filtered to isolate the frequency component of interest (this avoids the contamination of phase estimation by other frequency components); second, phase is estimated with high temporal resolution; third, a method is used to estimate the degree of phase synchronization. To isolate the low frequency components containing information about transitions between UP and DOWN states, all signals were processed with a discrete wavelet transformation (8) performed by a finite impulse response digital filter approximation of the Meyer wavelet function (MatLab, The MathWorks). The procedure works like an iterative band-pass filter that allows obtaining a family of waveforms retaining different frequency components of the original signal (for more details, see ref. 2; see also Fig. S2). The waveforms used in the present study contained frequency information within the 0.5–2 Hz band (as assessed from power spectra) and closely matched the time course of UP and DOWN states and LFP slow waves (see Fig. 2*A* to scrutiny the correspondence between raw signals and their 0.5–2 Hz wavelet component; see also figures 2 and 10 in ref. 2). "Instantaneous phases" (1-ms resolution) were estimated by performing a Hilbert transform on the 0.5–2 Hz frequency components of the V_m and LFPs (9). Then, we dissected the transitions to the UP and DOWN state.

Transitions were defined as zero crossing with a positive (DOWN to UP state) or negative (UP to DOWN state) slope within the normalized (-1 to 1) wavelet transformed 0.5–2 Hz V_m (2). Four hundred millisecond time windows centered at V_m transitions were cut from all of the wavelet transformed signals (V_m and LFPs). Within each 400 ms epoch, the mean direction of the circular distribution of phase differences between the V_m and each LFP was taken as the phase difference during the transition to the UP state (PDT) (ref. 10; Fig. S2). Thus, each MSN recording was in the end represented by three collections of 75–100 PDT (MSN-motor cortex LFP; MSN-sensory cortex LFP, MSN-cingulate cortex LFP). The circular dispersion of these collections of PDTs was taken as an index of phase locking. Mean directions and circular dispersions were calculated after ref. 10. Additionally, for each 400 ms UP state transition we estimated an "average PDT" by averaging the three PDTs (Fig. 2*C*).

Multivariate Statistics. Partial least squares (PLS) analysis is a multivariate statistical method used to analyze neuroimaging data and is popular in other scientific fields (11). PLS operates on the covariance between blocks of data to obtain a discrete number of "latent variables" that account for most of the variance. Thus, the latent variables describe the relation between blocks of data using the fewest dimensions. Here, PLS served to identify the patterns of corticostriatal functional connectivity that distinguished the three striatal regions. PLS entailed three computational steps (adapted from the "task PLS" of ref. 11). First, the correlation between data blocks representing functional connectivity (coherence) between V_m and LFPs and orthogonal (Helmert) contrasts was computed across the three striatal regions. Second, singular value decomposition was performed on the resulting matrix to generate the latent variables (here, two latent variables were obtained, as only two orthogonal contrast are possible between three striatal regions). In PLS each latent variable is associated with a "singular value" (which is proportional to the percentage of cross-block total covariance explained for by the latent variable), a "singular matrix" (an optimized description of the data based on the positive or negative covariation with the contrasts), and a singular profile (representing the weighted contribution of each experimental condition - striatal region - to the latent variable), The statistical confidence of singular values, which tells whether a given latent variable is relevant or not, was assessed by conducting PLS on 499 shuffled data blocks. Shuffling was done by reassigning randomly MSNs to striatal regions. The null hypothesis was rejected when the probability of finding a singular value equal or higher than that obtained from the original data block was less than 5%. In addition to testing the statistical significance of the latent variables, we assessed the reliability of values in the singular matrix (saliences) by evaluating the contribution of each striatal neuron to the pattern obtained within each striatal region. This was done with an iterative procedure involving randomly resampling individual cases from the original data matrix with replacement (bootstrapping), and then computing PLS on the modified data matrix. This was repeated 100 times, allowing expressing the distance between a salience and the population mean in standard error units, where a value of 2 means that the distance equals two standard errors from the mean, and the sign indicates whether it is above or below the population mean. Distances higher than 2 standard errors were considered significant. Weights in the singular profile take values between 1 and –1, have no units, and are not associated with a statistical dispersion measure. To allow scrutinizing the contribution of each subject (MSN) to the singular profile, subject scores are weighted by multiplying the original dataset by the singular matrix and plotted for each experimental condition (striatal region).

As PLS revealed significant effects of striatal regions on patterns of connectivity with the cortical areas, we did further comparisons within the striatal regions with one-way ANOVAs or the Kruskall–Wallis test.

1. Kasanetz F, Riquelme LA, Murer MG (2002) Disruption of the two-state membrane potential of striatal neurones during cortical desynchronisation in anaesthetised rats. *J Physiol* 543:577–589.
2. Kasanetz F, Riquelme LA, O'Donnell P, Murer MG (2006) Turning off cortical ensembles stops striatal Up states and elicits phase perturbations in cortical and striatal slow oscillations in rat in vivo *J Physiol.* 577:97–113.
3. Paxinos W (1997) in *The Rat Brain in Stereotaxic Coordinates* (Academic, London), 3rd Ed.
4. Tseng KY, Kasanetz F, Kargieman L, Riquelme LA, Murer MG (2001) Cortical slow oscillatory activity is reflected in the membrane potential and spike trains of striatal neurons in rats with chronic nigrostriatal lesions. *J Neurosci* 21:6430–6439.
5. Kita H, Armstrong W (1991) A biotin-containing compound N-(2-aminoethyl) biotinamide for intracellular labeling and neuronal tracing studies: comparison with biocytin. *J Neurosci Methods* 37:141–150.
6. Lopes da Silva F, Pijn JP, Boeijinga P (1989) Interdependence of EEG signals: linear vs. nonlinear associations and the significance of time delays and phase shifts. *Brain Topogr Fall-Winter;* 2:9–18.
7. Le Van Quyen M, Bragin A (2007) Analysis of dynamic brain oscillations: methodological advances. *Trends Neurosci* 30:365–373.
8. Meyer Y (1992) Wavelets and Operators, in *Cambridge Studies in Advanced Mathematics* (Cambridge Univ Press, Cambridge, UK), no 37.
9. Oppenheim AV, Schafer RW, Buck CK (1999) *Discrete-Time Signal Processing*, (Prentice Hall, Englewood Cliffs, NJ), 2nd Ed.
10. Fisher NI (1993) *Statistical Analysis of Circular Data* (Cambridge Univ Press, Cambridge, UK).
11. McIntosh AR, Bookstein FL, Haxby JV, Grady CL (1996) Spatial pattern analysis of functional brain images using partial least squares. *NeuroImage* 3:143–157.

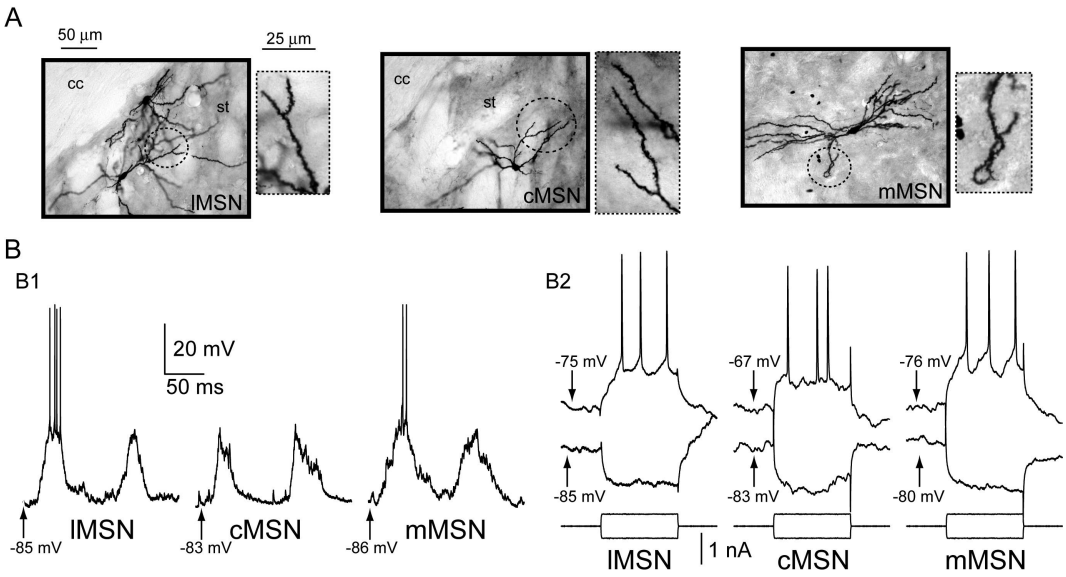

Fig. S1. (*A*) Microphotographs of MSNs labeled with Neurobiotin (cc: corpus callosum; st: striatum). (*Inset*) Dendritic spines magnified from encircled regions. (*B*) Representative recordings from MSNs in different striatal territories, showing the typical V_m two-state alternation (*1*) and responses to current steps applied at the soma (*2*). lMSN: rostrolateral MSN; cMSN: caudal MSN; mMSN: rostromedial MSN.

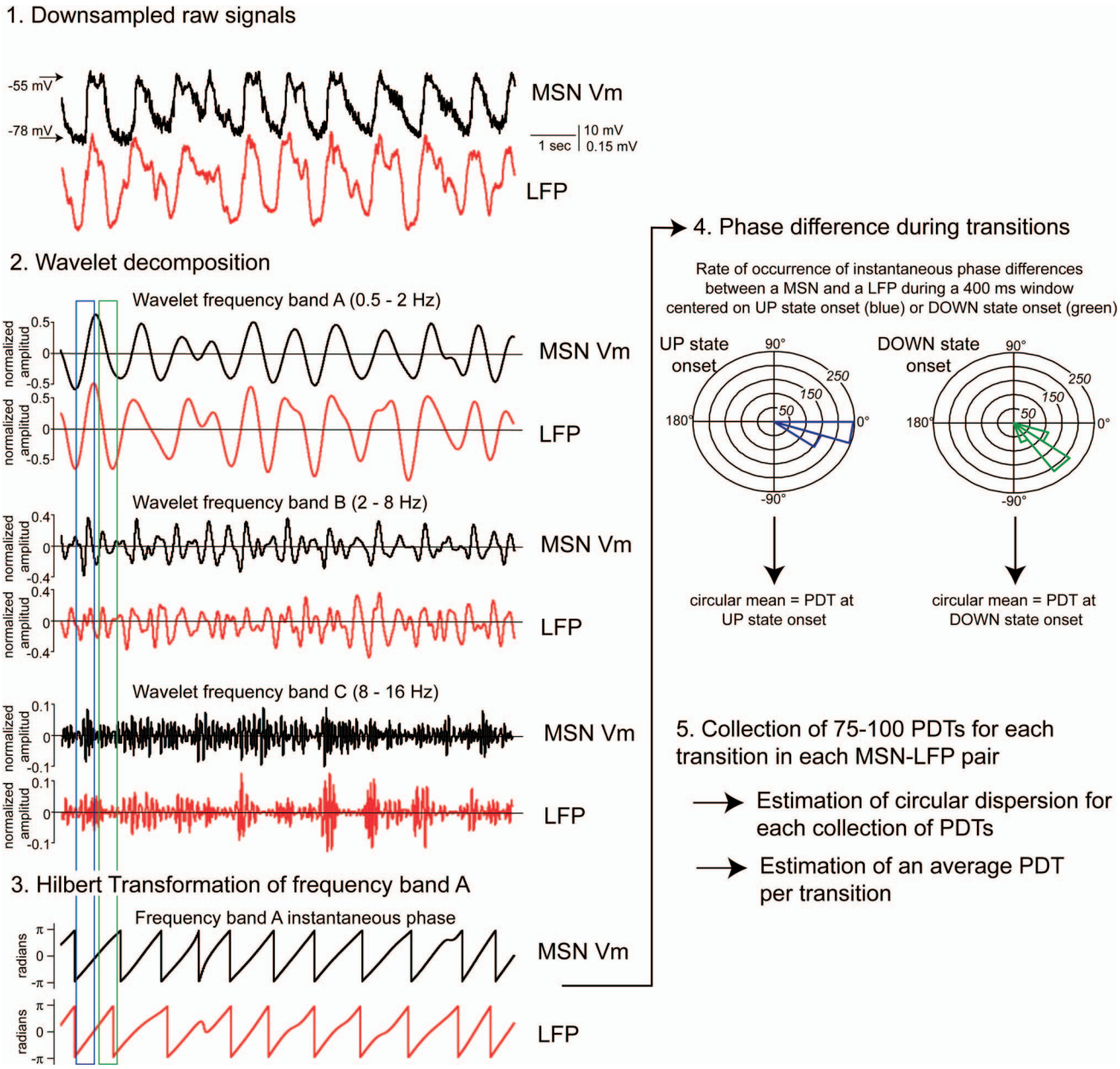

Fig. S2. Overview of method used for estimating PDT. (*1*) The raw signals were down-sampled and then amplitude normalized. Polarity in LFP is positive up. For simplicity, only one LFP recording is shown. (*2*) Wavelet decomposition allowed generating waveforms retaining different frequency components of each signal. The lowest frequency bands (0.5–2 Hz) retained information about the slow oscillation. The amplitude of the wavelet components reflects the power of the different frequencies in the original signals. Note that the power of the 8–16 Hz components increases during UP states and in coincidence with the positive (active) part of the LFP [see Kasanetz F, Riquelme LA, O'Donnell P, Murer MG (2006) Turning off cortical ensembles stops striatal Up states and elicits phase perturbations in cortical and striatal slow oscillations in rat in vivo *J Physiol.* 577:97–113, for the relationship between cortical LFP and local neuronal spiking]. (*3*) Estimation of phase in the low frequency components of the V_m and LFP with 1-ms resolution. (*4*) Taking as reference the 0.5–2 Hz wavelet component of the V_m, we used 400 ms time windows centered at UP state onset (zero crossing with positive slope; blue box) or UP state termination (zero crossing with negative slope; *green box*) all along the recordings. Within these windows, phase differences were computed with 1 ms resolution by subtracting the phase of the LFP from the phase in the MSN. Negative phase differences indicate that the MSN follows the LFP. The mean direction of the circular distribution of the 400 phase differences was taken as the ''phase difference at transition'' (PDT). (*5*) For each MSN, 75–100 UP states were studied, giving three collections (one per MSN-LFP pair) of 75–100 PDTs for transitions from DOWN to UP, and other three collections of 75–100 PDTs for transitions from UP to DOWN.

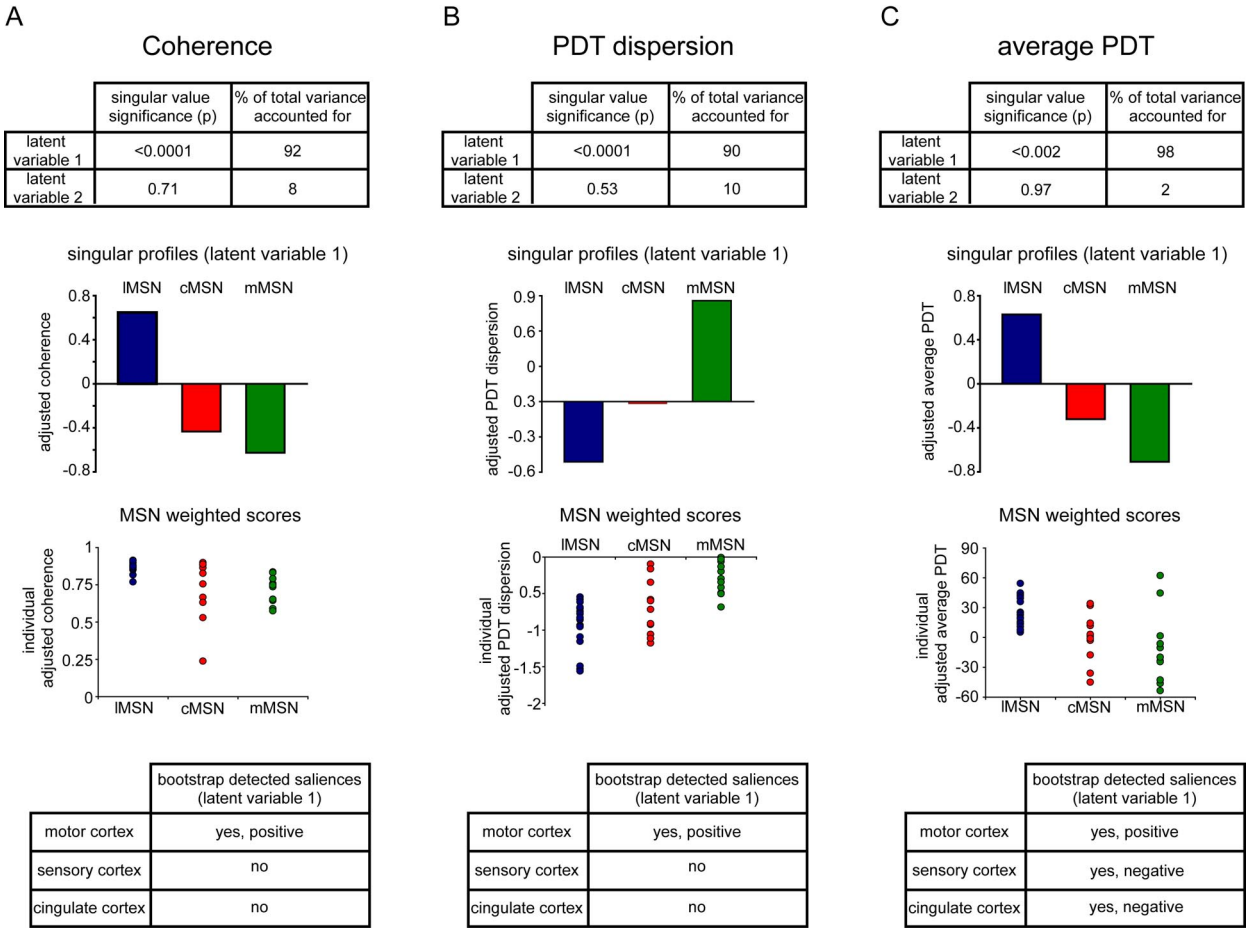

Fig. S3. Partial least squares (PLS) assessment of corticostriatal connectivity. With the aim of distinguishing the rostrolateral (lMSNs), caudal (cMSNs) and medial (mMSNs) striatum based on their association with different cortical areas, PLS was applied on two measures of functional connectivity, coherence (*A*) and PDT circular dispersion during transitions to the UP state (*B*). (*A*) When applied to coherence, PLS identified one significant latent variable. The singular profile identified a linear pattern of coherence between the different striatal regions and the motor cortex (as statistically identified with bootstrap), with higher coherence between the motor cortex and the rostrolateral striatum and lower coherence with the medial striatum. (*B*) PLS also identified a single significant latent variable in the PDT circular dispersion dataset of UP state onsets. The singular profile (same as in Fig. 3*B*) shows an inverse pattern to that obtained for the coherence. This is not unexpected, as coherence is directly related to the level of functional association between two regions and PDT is inversely related. Thus, here, the positive salience of the motor cortex indicates that the medial striatum had the highest and the rostrolateral striatum the lowest PDT dispersion. (*C*) PLS assessment of average PDTs during transitions to the UP state. The singular profile (same as in manuscript Fig. 4*B*) depicts the pattern of activation of the different striatal regions for waves led by each cortical area. Bootstrapping identified significant effects of the three cortical leading possibilities. Positive salience indicates a direct correlation between the singular profile and average PDT. Consequently, for motor cortex LFP leading, it means that lMSN reach the UP state sooner than mMSNs. The negative salience of cingulate cortex leading means that average PDT correlated negatively with the singular profile (so, average PDT was shorter in mMSN and longer in lMSN for waves initiated in the cingulate cortex). ''MSN weighted scores'' give an idea of the spread of the data and of the contribution of each MSN to the singular profile.

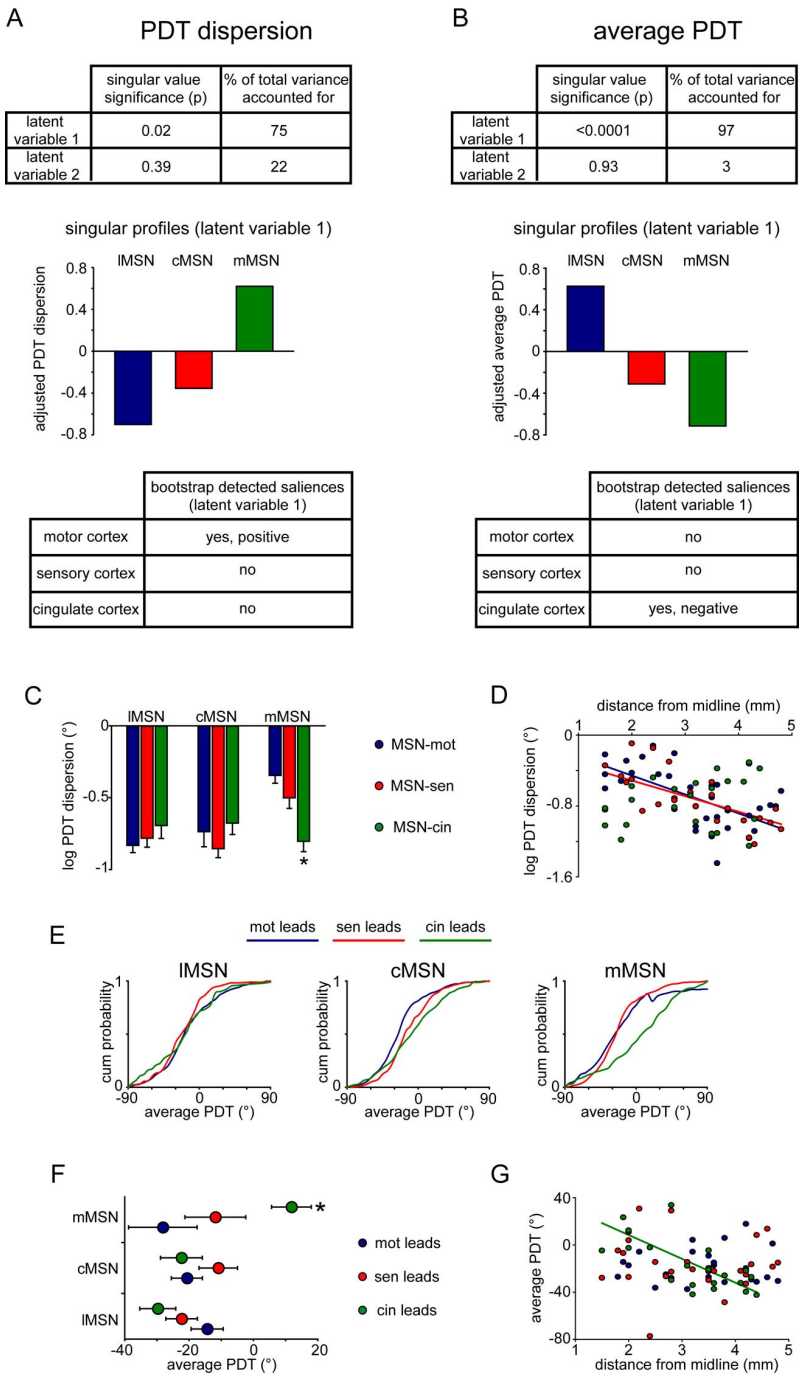

Fig. S4. Segregation during MSN transitions to the DOWN state. PDTs were calculated as described above and data analyzed as in transitions to the UP state. (*A* and *B*) PLS analysis of PDT dispersion (*A*) and average PDT (*B*) during transitions to the DOWN state. The singular profiles show patterns similar to those revealed in transitions to the UP state (compare with Fig. S3). (*C*) Circular dispersion of PDTs compared within MSN categories as in Fig. 3*C*. Significant differences were found only within mMSNs, which were more tightly locked to the cingulate than to any other LFP (*, $P < 0.01$ versus either motor or sensory LFPs, posthoc Holm Sidak test after significant repeated measures ANOVA). Overall, PDT dispersions were higher than for UP state onsets. (*D*) Linear relationship between MSN distance from midline and PDT dispersion for the motor (black line, regression ANOVA, $P < 0.001$, $r = 0.60$) and sensory LFPs (dashed line, regression ANOVA, $P < 0.005$, $r = 0.52$). (*C*) Cumulative frequency histograms of average PDTs (compare with Fig. 4*A*). (*D*) Comparisons of average PDTs within MSN categories (as in Fig. 4*C*). Significant differences were detected only in mMSNs, which reached the DOWN state earlier when the cingulate cortex led the transition (*, $P < 0.01$ versus motor or sensory, post hoc Holm Sidak). (*E*) Linear relationship between average PDT and MSN distance from midline when the cingulate LFP led transitions to the DOWN state (regression ANOVA, $P < 0.001$, $r = 0.71$). Overall, all of the variables behaved similarly during transitions to the UP or DOWN states.

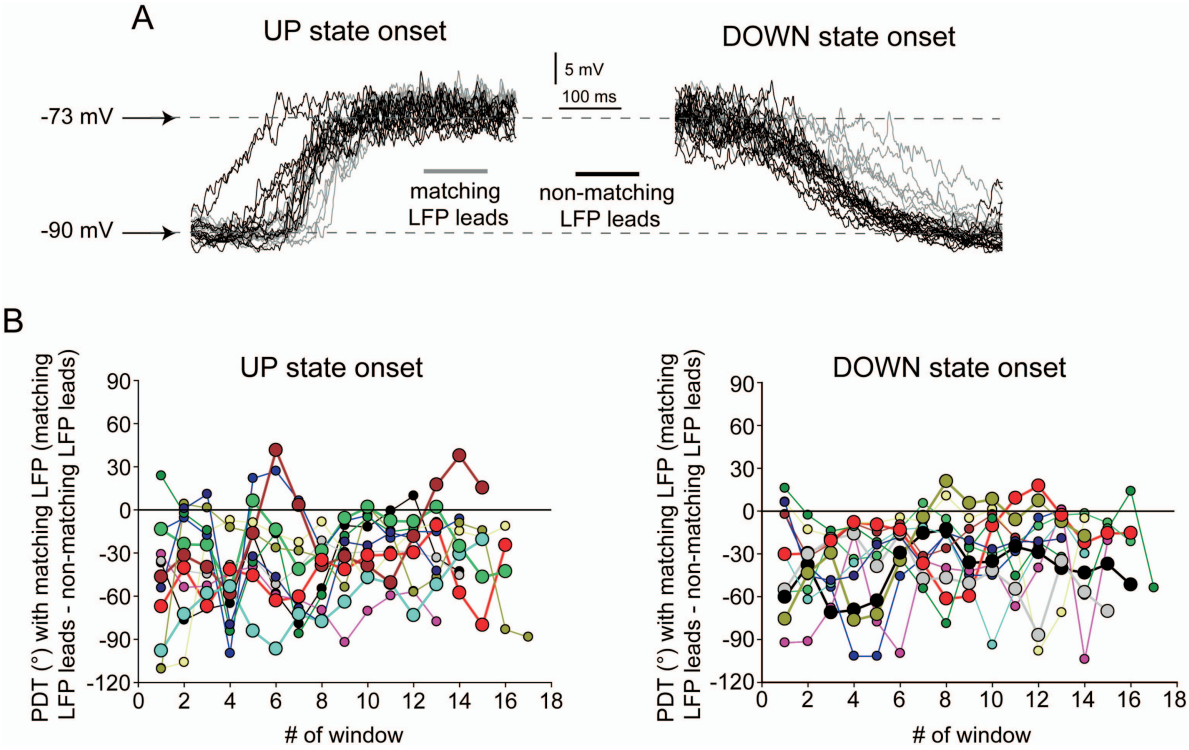

Fig. S5. Alternating patterns of propagation with overall steady cross-talk over time. (*A*) Representative transitions to the UP (*Left*) or DOWN (*Right*) state in a mMSN, relative to the cingulate LFP (aligned at the time of zero crossing), for cycles led by the cingulate (gray) or nonmatching (black) LFPs. (*B*) The PDT between a MSN and its matching LFP was studied with a sliding window spanning 10 transitions (50% overlap). Within each window, waves were separated in ''match'' and ''nonmatch'' leading and PDTs averaged within these two categories. Then, the mean PDT of nonmatch leadings was subtracted from the mean PDT of match leadings. This compensates for differences in the number of match versus non-match leadings within each window. Most window values being below zero indicates that PDT was higher when the matching LFP led (see also Fig. 5*B*). Each line corresponds to a MSN. In some neurons, cross-talk consistently influenced PDT along the entire 90-econd recording (see enlarged circles as examples: red and cyan in UP states onset and gray and black in DOWN state onset). In other cells, alternating windows with and without cross-talk were observed (see light green and brown in UP state onset and red and light brown in DOWN state onset). Every window had matching and non-matching leadings, implying a highly dynamic slow wave cortical activity.

Table S1. Electrophysiological properties of MSN

	lMSN	cMSN	mMSN
Membrane potential (mV), UP	-72.2 ± 2.4	-69 ± 3.6	-71.9 ± 2.3
Membrane potential (mV), DOWN	-87.2 ± 2.3	-80.9 ± 4	-87.3 ± 1.6
Input resistance measured with a hyperpolarizing step during the DOWN state (MΩ)	31.1 ± 2.9	33.3 ± 2.8	37.3 ± 3.9
Input resistance measured with a depolarizing step during the DOWN state (MΩ)	38.3 ± 2.8*	40.1 ± 4.1*	48.5 ± 3.8*
Firing rate (spikes per second)	0.32 ± 0.16	0.33 ± 0.19	0.3 ± 0.22

*$P<0.05$, Student's paired *t* test between input resistances measured with hyperpolarizing or depolarizing current steps.